Research Article

Chemical Review and Letters
journal homepage: www.chemrevlett.com
ISSN (online): 2645-4947 (print) 2676-7279

DFT Investigation of Structure, stability, NBO charge on Titanium-Nitrogen Nanoheterofullerenes evolved from a small nanocage

Iman Sabeeh Hasan[1], Alhussein Arkan Majhool [2], Mustafa Humam Sami [3], Mohaned Adil [4], Saripah Salbiah Syed Abdul Azziz [5]

[1] *Department of Pharmacy, Al-Zahrawi University College, Karbala, Iraq*
[2] *College of Applied Medical Sciences, University of Kerbala, Kerbala, Iraq*
[3] *Department of Pharmacy, Al-Noor University College, Nineveh, Iraq*
[4] *Medical technical college, Al-Farahidi University, Iraq*
[5] *Chemistry Department, Faculty of Science and Mathematics, Sultan Idris Education University, 35900, Tanjong Malim, Perak, Malaysia*

ARTICLE INFO

Article history:
Received 8 April 2023
Received in revised form 26 July 2023
Accepted 26 July 2023
Available online 26 October 2023

Keywords:
Heterofullerene
Heteroatom
Stability
NICS
NBO

ABSTRACT

In this DFT (density functional theory) approach, we are performed geometric and electronic properties of Ti—N hallow cages improved from C_{20} *i.e.*, $C_{20-2n}Ti_nN_n$ (n = 1-8), at (U)B3LYP, (U)M062X, (U)B3PW91//6-311++G**, AUG-cc-pVTZ. Except for $C_4Ti_8N_8$, other structures are real minima and none deform as segregated open cage. Substituting causes different $\Delta E_{HOMO-LUMO}$ values (the frontier molecular orbital energy separation) and $C_{18}Ti_1N_1$ is distinguished as the suitable insulated structure, while $C_{12}Ti_4N_4$ is considered as the proper conductive structure. There is good reliability among polarizability, and ionization potential with substituting Ti—N units. The NICS (0) shows aromaticity decreases as n increases. Due to eight Ti—N units in the symmetrical positions of $C_4Ti_8N_8$ cage, it shows dipole moment of 0.00 Debye, and the smallest charge of +0.526 on Ti. Considering the least $|E_{ads.}|$; $|-18.9$ kcal/mol$|$; and the greatest charge of +1.269 on titaniums of $C_{18}Ti_1N_1$, it is recommended for hydrogen storage. The NBO of $C_{18}Ti_1N_1$ points out higher intramolecular charge transfer (ICT) from donor orbitals to acceptor orbitals through the appropriate overlapping between $LP(1)_N \rightarrow \pi^*_{C=C}$, $\pi_{C=C} \rightarrow \sigma^*_{C—Ti}$, $\pi_{C=C} \rightarrow \sigma^*_{C—Ti}$, $\sigma_{C—Ti} \rightarrow \pi^*_{C=C}$ and $LP(1)_N \rightarrow \sigma^*_{C—Ti}$ orbitals of $C_{18}Ti_1N_1$.

1. Introduction

The C_{20} is comprising pentagons with great curvature. Due to interesting construction of this hollow cage, it has been subject of many theoretical surveys [1-7]. Initially, interaction of C_{20} with the lithium heteroatom does not give significant modification in the cage geometry. It is inspected to be more reactive than it's bowl and ring analogue, even though the relative energy among these isomers is influenced by sophistication of the applied theoretical methods [1-7]. It is distinguished as the most stable twenty vertex polyhedral with the minimum energy amid the mathematically probable fullerenes. From an experimental point of view, this fullerene produced through stable $C_{20}H_{20}$ in gas phase [8].Furthermore, the synthesis and the doped nanosheets can be confirmed with some categorizations. Moreover, encapsulation of metal−endohedral fullerenes such as Ti@C_{28}, Zr@C_{28}, and U@C_{28} are investigated *via* a bottom-up growth process [8-13]. The substituted aluminum and/or titanium heteroatoms stabilize the highly strained C_{20}, C_{24}, C_{28} fullerenes *via* charge transfer (CT) from the electropositive dopant to carbon [14]. Regardless of Ti—decorated boron cages that B_{38} and B_{40} have been achieved as the first experimentally full-heterofullerene, H_2 storage of the designed transition metals at heptagon and hexagon rings of these structures have been surveyed through DFT [15].

∗ Corresponding author.; e-mail: shadaldlymy747@gmail.com
https://doi.org/ 10.22034/CRL.2023.392371.1223

Experimental and theoretical inspections have revealed that Ti—clusters significantly improve H_2 storage [15]. Our enquiry further proofs theoretical insight into substituent effect of Ti—N units on $C_{20-2n}Ti_nN_n$ structures, to respect which of them are suitable for H_2 storage (Figure 1).

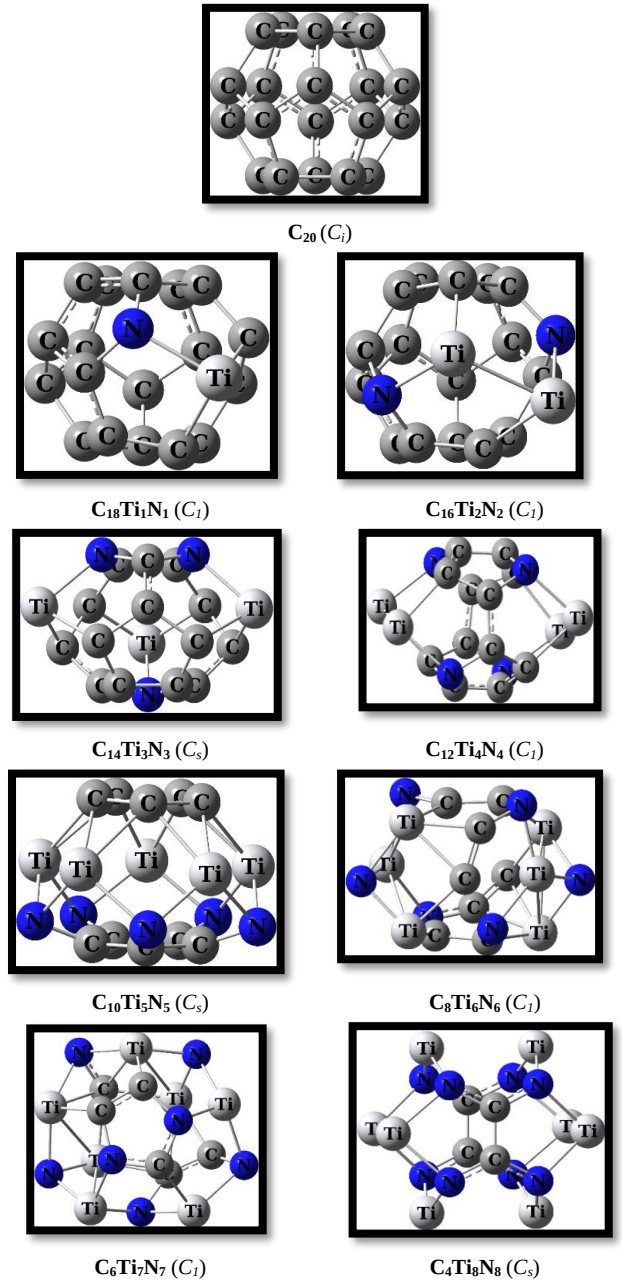

Fig. 1. The optimized **C_{20}** and its derivatives as well as their point groups, at B3LYP/AUG-cc-pVTZ.

2. Computational Methods

The optimization is done for closed-shell multiplicity (n = 0, 2, 4, 6, 8) at the restricted spin-symmetry methods and for opened-shell multiplicity (n = 1, 3, 5, 7) at the unrestricted spin-symmetry methods using the GAMESS [16-18]. Harmonic frequencies are obtained to realize nature and ZPVE value [18]. The NBO [19], aromaticity [20], MEP as well as reactivity [21] calculations are individually achieved, at three methods. The reactivity is accomplished *via* $N = E_{HOMO(Nu)} - E_{HOMO(tetracyanoethylene)}$, $\omega = \mu^2 / 2\eta$, $\mu = (E_{HOMO} + E_{LUMO}) / 2$, $\eta = (E_{LUMO} - E_{HOMO}) / 2$, $\chi = -\mu$, $S = 1 / 2\eta$, and $\Delta N_{max} = -\mu / \eta$.

3. Results and Discussion

In the succeeding parts we will discuss substituted heteroatom effects by increasing the Ti—N units, however there are many other likely isomers but we are investigated eight of them.

3.1.Structural investigation

The structures of studied molecules are explained in terms of bond distances close to the substituting elements. The C—C bond distances of **C_{20}** are around 1.44 – 1.54 Å (Tables 1 and 2) which insert amid the values of $H_2C{=}CH_2$ and $H_3C{-}CH_3$ (1.35 and 1.54 Å, respectively).

Table 1. The bond lengths per Å, at B3LYP/AUG-cc-pVTZ.

Species	C=C	Ti–C	N–C
C_{20}	1.444-1.537	-	-
$C_{18}Ti_1N_1$	1.398-1.538	1.444	1.443
$C_{16}Ti_2N_2$	1.410-1.523	2.006-2.021	1.408-1.432
$C_{14}Ti_3N_3$	1.397-1.501	1.877-2.074	1.424-1.491
$C_{12}Ti_4N_4$	1.402-1.493	1.079-2.080	1.395-1.448
$C_{10}Ti_5N_5$	1.402-1.523	1.587-1.609	1.587-1.609
$C_8Ti_6N_6$	1.336-1.482	1.943-2.165	1.355-1.488
$C_6Ti_7N_7$	1.408-1.414	2.117-2.162	1.376-1.419
$C_4Ti_8N_8$	1.449	-	1.375

Table 2. The bond lengths per Å, at B3LYP/AUG-cc-pVTZ.

Species	Ti–N	Ti–Ti
C_{20}	-	
$C_{18}Ti_1N_1$	1.442	-
$C_{16}Ti_2N_2$	2.006-2.027	2.380
$C_{14}Ti_3N_3$	1.953-1.984	-
$C_{12}Ti_4N_4$	2.041-2.065	2.305
$C_{10}Ti_5N_5$	1.674-1.697	-
$C_8Ti_6N_6$	1.882-2.031	2.502-2.775
$C_6Ti_7N_7$	1.872-2.078	2.701-2.798
$C_4Ti_8N_8$	1.873-2.028	2.360

The considered Ti—C, and N—C bond lengths are expanded to approximately 1.77 - 2.61 Å which are followed with sum of covalent radii of the scrutinized atoms; C = 0.70 Å, Ti = 1.40 Å and N = 0.65 Å. Shrinking 0.11 Å in C═C bond length of heterofullerenes *vs.* **C_{20}** is attributed to dopants. The bond angles of C–Ĉ–C (99.59° – 118.82°), C–Ti–C (37.03° – 91.73°), and C–N–C (98.74° – 113.96°) are changed *vs.* C–Ĉ–C (103.99° to 111.31°) of pure **C_{20}** (Table 3).

Table 3. The bond angles (in degree), at B3LYP/AUG-cc-pVTZ.

Species	C–C–C	C–Ti–C	C–N–C
C_{20}	103.99-111.31	-	-
$C_{18}Ti_1N_1$	103.46-117.93	85.79	101.64
$C_{16}Ti_2N_2$	99.59-118.82	-	99.81-99.94
$C_{14}Ti_3N_3$	103.75-132.89	83.81-117.40	89.89-105.85
$C_{12}Ti_4N_4$	99.78-114.38	-	98.74-99.63
$C_{10}Ti_5N_5$	107.33-108.77	38.92-39.89	-
$C_8Ti_6N_6$	-	37.03-74.44	104.66-113.96
$C_6Ti_7N_7$	-	91.73	108.16
$C_4Ti_8N_8$		-	-

These variations create pyramidalization on dopant sites; $\theta_C = 360 - [(C–C–C)_1 + (C–C–C)_2 + (C–C–C)_3]$, $\theta_{Ti} = 360 - [(C–Ti–C)_1 + (C–Ti–N)_2 + (N–Ti–C)_3]$ and $\theta_N = 360 - [(C–N–C)_1 + (C–N–Ti)_2 + (Ti–N–C)_3$ (Table 4) [22-25].

Table 4. The pyramidalization angles of θ_{Ti}, θ_N (in degree), at B3LYP/AUG-cc-pVTZ. The pyramidalization angle of **C_{20}** is 31.623 - 42.254°.

Species	θ_{Ti}	θ_N
C_{20}	31.62-42.25	-
$C_{18}Ti_1N_1$	100.95	40.84
$C_{16}Ti_2N_2$	64.22	35.5
$C_{14}Ti_3N_3$	26.25-98.52	34.28-101.16
$C_{12}Ti_4N_4$	72.33-123.25	32.06-49.44
$C_{10}Ti_5N_5$	-	-
$C_8Ti_6N_6$	-	35.32-115.38
$C_6Ti_7N_7$	23.39-71.26	40.86-92.14
$C_4Ti_8N_8$	76.85	40.23

Here, the substituting dopants of $C_{20-2n}Ti_nN_n$ species displays more pyramidalization *vs.* C_{20}, owing to their more tendency to accept sp^3 hybridization than sp^2. The smallest vibrational frequency (υ_{min}) analysis displays one negative frequency only for $C_4Ti_8N_8$ as transition state and positive frequencies for others as real minima (Table 5 and Figure 2).

Table 5. The total energy, smallest vibrational frequency, polarizability, and polarity.

Species	E_{tot}[a, (b), c, [d]] / *a.u.*	υ_{min}[e] / cm^{-1}	$<\alpha>$[b]	μ[b]
C_{20}	-761.60234 (-761.18425) -761.18350 [-761.67038]	82.23	187.27	0.00
$C_{18}Ti_1N_1$	-1589.47147 (-1589.11869) -1589.35354 [-1589.77347]	127.09	184.04	5.96
$C_{16}Ti_2N_2$	-2417.44789 (-2417.12013) -2417.33158 [-2417.83232]	104.94	243.27	5.95
$C_{14}Ti_3N_3$	-3245.52935 (-3245.15983) -3245.35522 [-3245.95661]	137.84	250.89	5.64
$C_{12}Ti_4N_4$	-4073.41358 (-4073.102759) -4073.29079 [-4073.953506]	75.13	483.89	0.54
$C_{10}Ti_5N_5$	-4901.89785 (-4901.57717) -4901.77369 [-4902.461001]	158.28	298.21	4.37
$C_8Ti_6N_6$	-5729.82262 (-5729.56165) -5729.68969 [-5730.50202]	109.37	304.89	3.12
$C_6Ti_7N_7$	-6557.772910 (-6557.71081) -6557.84980 [-6558.02788]	91.56	398.25	1.54
$C_4Ti_8N_8$	-7386.224877 (-7385.58105) -7385.68065 [-7385.81647]	-269.67	633.14	0.00

At [a]B3LYP/6-311++G**, [b]M06-2X/6-311++G**, [c]B3PW91/6-311++G**, [d]B3LYP/AUG-cc-pVTZ, and [e]B3LYP/6-311+G*.

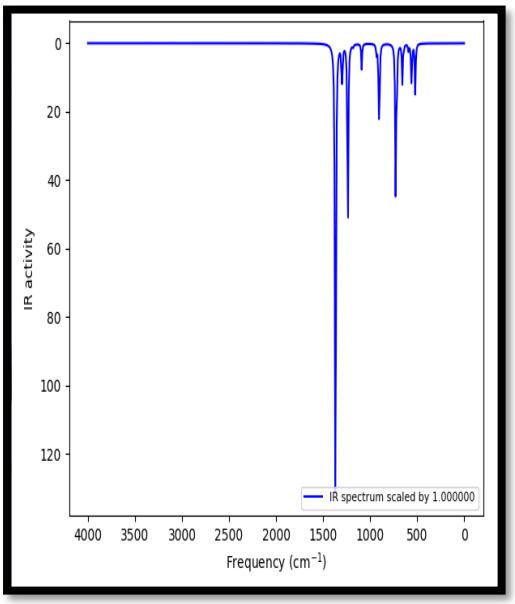

C_{20}

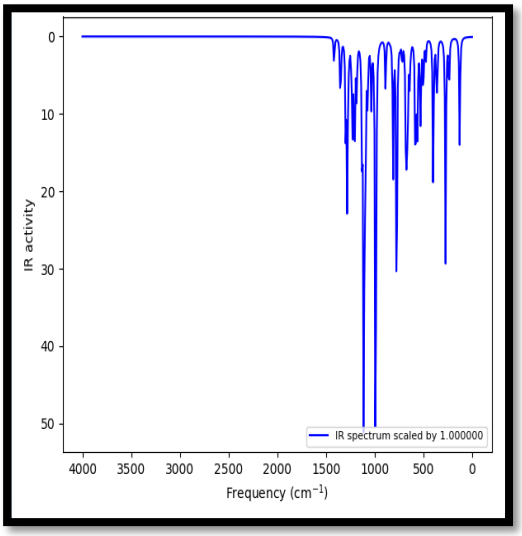

$C_{18}Ti_1N_1$

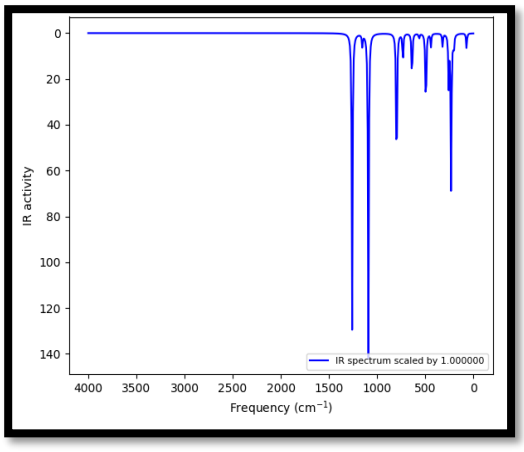

$C_4Ti_8N_8$

Fig. 2. The selected IR spectrum of C_{20}, $C_{18}Ti_1N_1$ and $C_4Ti_8N_8$, at B3LYP/6-311+G*.

Here, the E_{tot} is increased as n is increased and $C_{18}Ti_1N_1$, $C_{16}Ti_2N_2$, $C_{10}Ti_5N_5$, and $C_8Ti_6N_6$ structures compare to C_{20} fulfill "stability conditions" showing the υ_{min} values of 127.09, 104.94, 158.28, and 109.37 cm^{-1}, which are high *vs.* 82.2 cm^{-1} [26]. Interestingly, there is good consistency between <α> and the order of n. The <α> is improved from 187.27 *a.u.* for C_{20} to 633.14 *a.u.* for $C_4Ti_8N_8$. It seems that the substituted Ti, N heteroatoms in $C_{20-2n}Ti_nN_n$ heterofullerens lead to increasing <α> and $C_4Ti_8N_8$ has more tendency to interaction with the neighboring polar molecule. The substituted doping C_{20} to $C_{18}Ti_1N_1$, $C_{16}Ti_2N_2$, $C_{10}Ti_5N_5$, $C_8Ti_6N_6$, and $C_6Ti_7N_7$ is caused considerably μ of 5.96, 5.96, 4.37, 3.12, and 1.54 Debye, respectively (Table 5).

3.2. $\Delta E_{HOMO\text{-}LUMO}$, IE or IP, and NICS

One Ti—N bond of $C_{18}Ti_1N_1$ is increased the $\Delta E_{HOMO\text{-}LUMO}$ (1.79, 2.06, 1.80 eV) leading to enhanced stability against electronic excitations (Table 6).

Table 6. The FMO (in *a.u.*), along with band gap (in eV).

Species	E_{HOMO}[a, (b), [c]]	E_{LUMO}[a, (b), [c]]	$\Delta E_{HOMO\text{-}LUMO}$[a, (b), [c]]
C_{20}	-0.20134 (-0.21055) [-0.20455]	-0.13054 (-0.12567) [-0.13351]	1.93 (2.31) [1.93]
$C_{18}Ti_1N_1$	-0.19002 (-0.19519) [-0.19241]	-0.15070 (-0.11964) [-0.12624]	1.79 (2.06) [1.80]
$C_{16}Ti_2N_2$	-0.17362 (-0.18059) [-0.17470]	-0.11566 (-0.11286) [-0.11676]	1.58 (1.84) [1.58]
$C_{14}Ti_3N_3$	-0.19181 (-0.14289) [-0.13560]	-0.13945 (-0.07834) [-0.08806]	1.42 (1.76) [1.29]
$C_{12}Ti_4N_4$	-0.13989 (-0.13985) [-0.13950]	-0.10388 (-0.10964) [-0.10395]	0.98 (0.82) [0.97]
$C_{10}Ti_5N_5$	-0.17146 (-0.17086) [-0.17365]	-0.10626 (-0.10488) [-0.10643]	1.77 (1.80) [1.83]
$C_8Ti_6N_6$	-0.14359 (-0.14230) [-0.14680]	-0.08387 (-0.08321) [-0.07701]	1.63 (1.61) [1.20]
$C_6Ti_7N_7$	-0.14090 (-0.14088) [-0.14581]	-0.09408 (-0.09672) [-0.10790]	1.27 (1.20) [1.03]
$C_4Ti_8N_8$	-0.13346 (-0.13258) [-0.12279]	-0.08443 (-0.08651) [-0.08700]	1.33 (1.25) [0.97]

At [a]B3LYP/AUG-cc-pVTZ, [b]M06-2X/6-311++G**, and [c]B3PW91/6-311+G*.

Four Ti—N bonds of $C_{12}Ti_4N_4$ are decreased the $\Delta E_{HOMO\text{-}LUMO}$ of 0.98 eV at B3LYP/AUG-cc-pVTZ, 0.82 eV at M06-2X/6-311++G**, 0.97 eV at B3PW91/6-311+G* and leading to the enhanced conductivity of $C_{12}Ti_4N_4$. Hence, $C_{18}Ti_1N_1$ is distinguished as the most kinethic stable derivative, whereas $C_{12}Ti_4N_4$ with four separated Ti—N units *via* four C═C bonds is classified as the least kinethic stable one. Also, we are evaluated the ionization energy or ionization potential (IE or IP) (Table 7). Now, to probe proper connection, we compare $\Delta E_{HOMO\text{-}LUMO}$, IE or IP, and aromaticity based on $|NICS\ (0)|$ of C_{20} and heterofullerenes with n. The $\Delta E_{HOMO\text{-}LUMO}$ value of heterofullerenes is lower than that of C_{20}, and there is no uniformity amid band gap and n (Figure 3).

Table 7. The ionization potential, and NICS (0), at B3LYP/AUGcc-pVTZ.

Species	IE (IP)	NICS (0)	NICS (0)$_{zz}$
C_{20}	167.75	-23.81	3.69
$C_{18}Ti_1N_1$	162.07	-42.05	-60.98
$C_{16}Ti_2N_2$	156.31	-37.82	-52.03
$C_{14}Ti_3N_3$	150.81	-19.50	-35.12
$C_{12}Ti_4N_4$	145.09	-15.72	-55.32
$C_{10}Ti_5N_5$	139.42	-13.51	-40.83
$C_8Ti_6N_6$	133.69	-19.94	-30.89
$C_6Ti_7N_7$	127.74	-13.42	-16.05
$C_4Ti_8N_8$	121.87	-16.10	-25.16

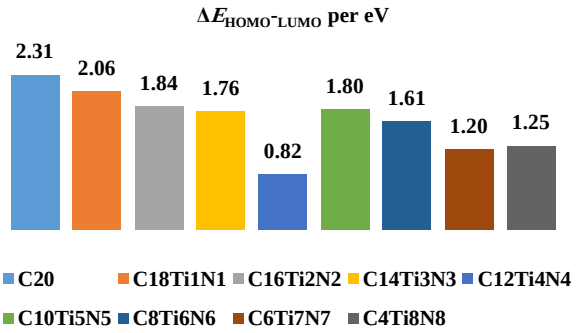

Fig. 3. The relationship between band gap and n, at B3LYP/AUG-cc-pVTZ.

The formations of these nanocages are quite complicated due to the possibility of high-spin states. Such possibilities arise due to insertion of Ti ($^3F_2$) and N ($^4S_{3/2}$) of atoms in C_{20}. The band gap values reveal different electronic charge-transfer possibilities within the considered molecules, while Ti—N units are increased in the fullerenes. The IE or IP value of $C_{20\text{-}2n}Ti_nN_n$ heterofullerens is decreased with increasing n (Figure 4).

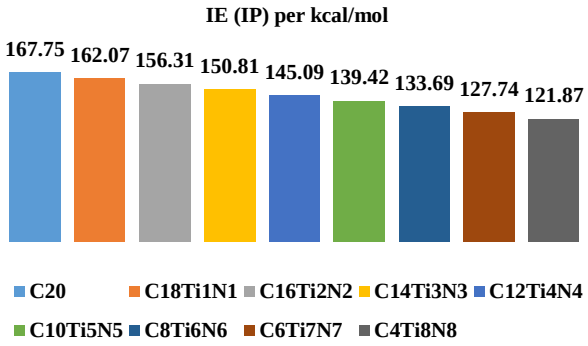

Fig. 4. The relationship between ionization potential and n.

We are obtained isotropic parameter of -23.8 ppm for C_{20}, which indicates strong aromaticity of it *vs.* benzene (-8.5 ppm) (Table 7). The $C_{20\text{-}2n}Ti_nN_n$ heterofullerenes show different NICS (0) from -42.05 to -13.42 ppm and they are aromatic. Furthermore, the studied heterofullerenes exhibit NICS (0)zz from -60.98 ppm for $C_{18}Ti_1N_1$ to -16.05 ppm for $C_6Ti_7N_7$ which imply strong ring current *vs.* benzene (-10.17 ppm). With increasing n, the delocalized π-electrons are shifted from more Ti heteroatoms to neighboring atoms (Figure 5).

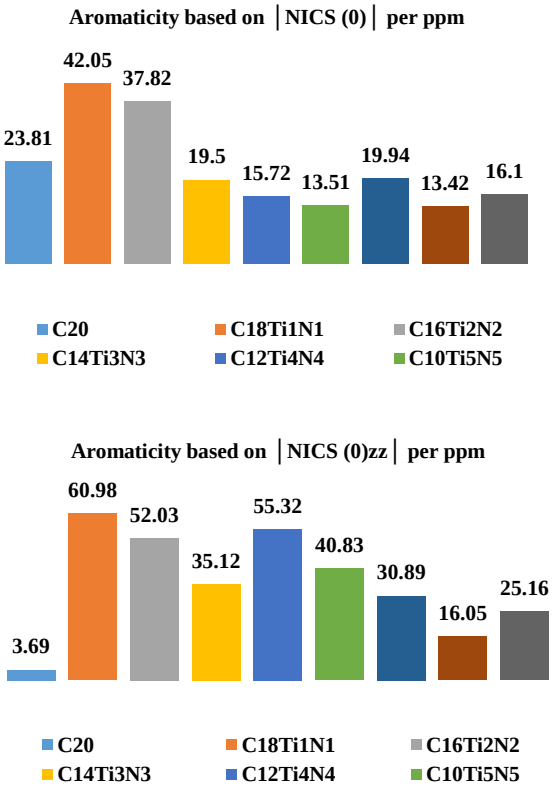

Fig. 5. The relationship between aromaticity and n.

Even though the electronegativity difference is significant, π-delocalization effect on the ring perimeter is strengthened in **$C_{18}Ti_1N_1$** derivative, while such ring current is weakened in other

derivatives. Thus, the isotropic polarizability <α> is modified depending on n and dopant topology (Figure 6).

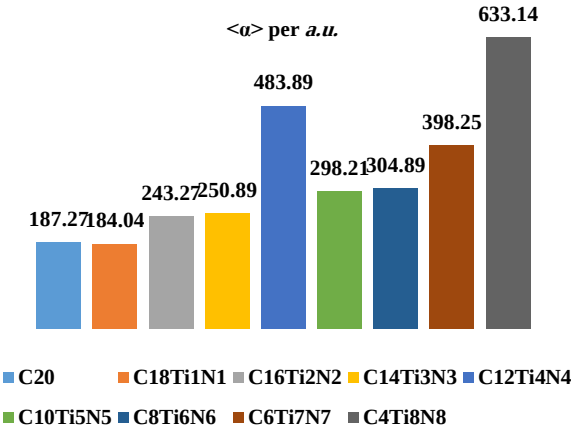

Fig. 6. The relationship between polarizability and n.

3.3. NBO charge, MEP, and hydrogen adsorption

Obviously, the NBO charges of derivatives are not equivalent; so that the negative charge on N sites is changed from −0.973 to −0.589e and the positive charge on Ti sites is improved from +0.527 for $C_4Ti_8N_8$ to +1.269 for $C_{18}Ti_1N_1$ (Figure 7).

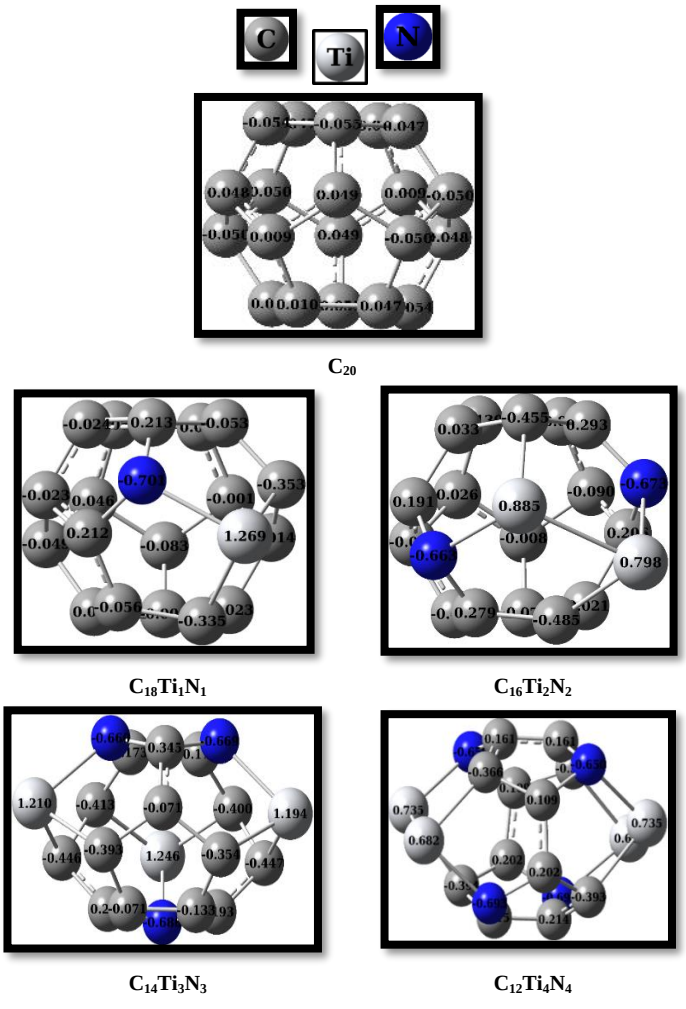

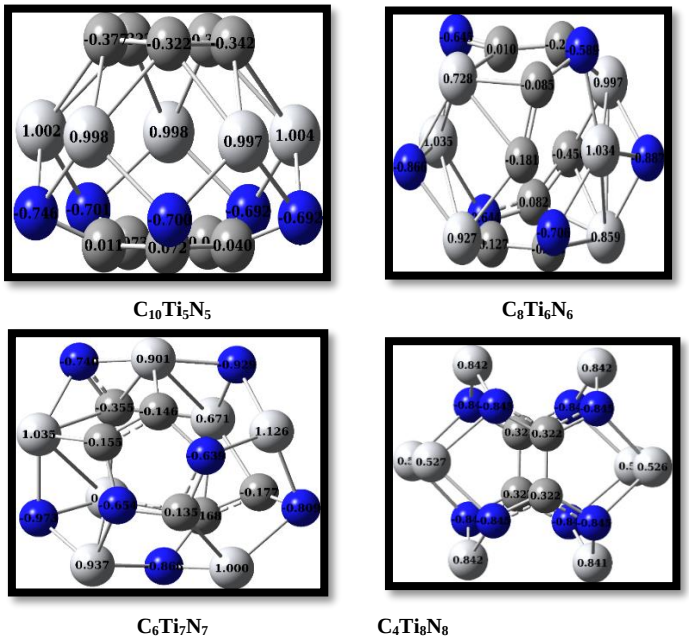

Fig. 7. The NBO charge on atoms of C20 and heterofullerenes, at B3PW91/6-311++G**.

Based on Froudakis's findings, $C_{18}Ti_1N_1$ is as the suggested species for H_2 storage [23]. The MEP is displayed though red—blue colors on Ti—N surfaces indicating their dispersed charges, correspondingly (Figure 8).

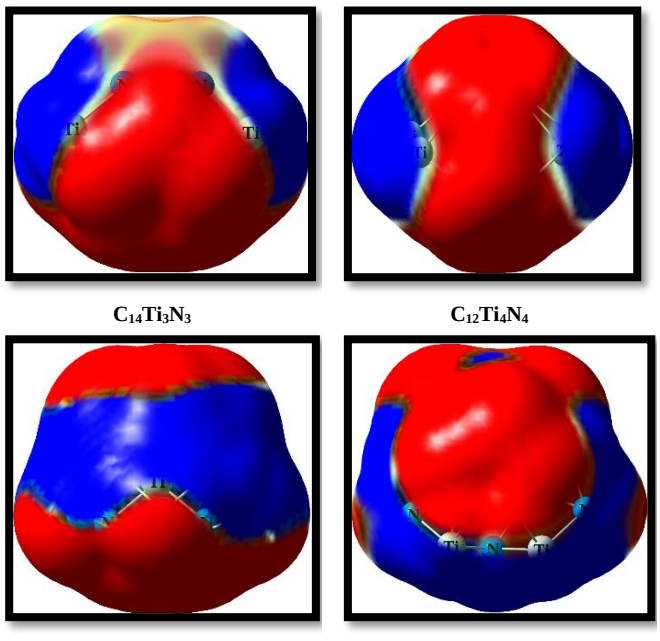

Fig. 8. Three-dimensional MEP of the selected derivatives, at B3PW91/6-311++G**.

We are probed H_2 adsorption on one to eight Ti and N–modified heterofullerenes using DFT simulations to introduce suitable systems for the storage of H_2 molecules. We have not used number of the Ti and N heteroatoms more than eight in C_{20}; because the optimized heterofullerenes with the molecular formula of $C_{20-2n}Ti_nN_n$ (n > 8) are collapsed to the segregated open cage structures. The mixed transition metal

(titanium) and the main element of the periodic table (nitrogen with more electronegative than boron element) have been chosen, because the results of previous studies displayed that the interaction between H_2 molecules and Ti−decorated B_{38} and B_{40} fullerenes as the modified adsorbent materials are stronger than those of the other transition metals modified systems [13]. The hydrogen adsorption is designed by reaction of $C_{20-2n}Ti_nN_n + 2H_2 \rightarrow C_{20-2n}Ti_nN_n.....(H_2)_2$. The overall trend of $|E_{ads.}|$ (in kcal/mol) for two H_2 molecules is arranged as $C_4Ti_8N_8$ $|-33.20|$ > $C_6Ti_7N_7$ $|-31.04|$ > $C_8Ti_6N_6$ $|-29.41|$ > $C_{10}Ti_5N_5$ $|-27.54|$ > $C_{12}Ti_4N_4$ $|-25.72|$ > $C_{14}Ti_3N_3$ $|-23.22|$ > $C_{16}Ti_2N_2$ $|-21.08|$ > $C_{18}Ti_1N_1$ $|-18.9|$ *vs.* C_{20} (+81.1). Next, the theoretical work needs to be supported more in its theoretical form. Thus, we are added n H_2 to the titanium and nitrogen heteroatoms. Compared to $1Ti/B_{38}/(H_2)_1$ complex with capacity of 2.56 wt% and $|E_{ads.}|$ of 0.22 eV/H_2; here $C_{20-2n}Ti_nN_n$ systems show higher capacity. Each Ti—N unit can bind up to $2H_2$ with $|E_{ads.}|$ of 0.07 eV/H_2. For example, additional $10H_2$ molecules can be absorbed to $10H_2/C_{10}Ti_5N_5$ complex with capacity of 4.48 wt% and $|E_{ads.}|$ of 0.37 eV/H_2. Hence, the net NBO positive charge of the Ti heteroatom is decreased from +1.269 to +0.6680 also, the net NBO negative charge of the nitrogen heteroatom is decreased from $|-0.701e|$ to $|-0.232e|$.

3.4.Reactivity

Substituting of Ti—N units is led to various modifications of N, ω, μ, η, χ, S, and ΔN_{max} (Table 8).

Table 8. The reactivity parameters (in eV), at M06-2X/6-311++G**.

Species	N	ω	μ	η	χ	S	ΔN_{max}
C_{20}	3.73	4.53	-4.57	2.31	4.57	0.22	1.98
$C_{18}Ti_1N_1$	4.15	4.46	-4.28	2.06	4.28	0.24	2.08
$C_{16}Ti_2N_2$	4.55	4.32	-3.99	1.84	3.99	0.27	2.17
$C_{14}Ti_3N_3$	5.57	2.58	-3.01	1.76	3.01	0.28	1.71
$C_{12}Ti_4N_4$	5.65	7.01	-3.39	0.82	3.39	0.61	4.13
$C_{10}Ti_5N_5$	4.81	3.92	-3.75	1.80	3.75	0.28	2.09
$C_8Ti_6N_6$	5.59	2.93	-3.07	1.61	3.07	0.31	1.91
$C_6Ti_7N_7$	5.63	4.35	-3.23	1.20	3.23	0.42	2.69
$C_4Ti_8N_8$	5.85	3.54	-2.98	1.25	2.98	0.40	2.38

Regardless $C_{10}Ti_5N_5$, N is increased nearly with increasing n (from 3.73 eV for C_{20} *vs.* 4.15 eV for $C_{18}Ti_1N_1$ to 5.85 eV for $C_4Ti_8N_8$). Moreover, three, and four substituted Ti—N unit structure is the least, and most electrophile species (2.58, and 7.01 eV for $C_{14}Ti_3N_3$, and $C_{12}Ti_4N_4$, respectively, *vs.* 4.53 eV for C_{20}). $C_{18}Ti_1N_1$ contains the minimum N, S, and the maximum χ, η, and absolute μ among eight analogues. In contrast, $C_{12}Ti_4N_4$ includes the least η and the most ω, S, and ΔN_{max}. Hence, $C_{18}Ti_1N_1$, and $C_{12}Ti_4N_4$ are the least, and the most chemically reactive species, singly. The lowest and the highest positive ΔN_{max} is demonstrated for $C_{14}Ti_3N_3$ and $C_{12}Ti_4N_4$ as the weakest and the strongest electron acceptor from other donors.

3.5. NBO analysis

Here, we are focused on NBO analysis of $Ti_1N_1C_{18}$ species (Tables 9 and 10).

Table 9. The occupancy of the intramolecular bonds in $Ti_1N_1C_{18}$, at M06-2X/6-311++G**.

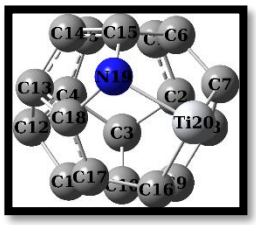

Bond	Occup.	ED_A (%)	ED_B (%)
$\pi_{C3=C10}$	0.74318	43.41	56.59
$\sigma_{C7—Ti20}$	0.86892	47.47	52.53
$\sigma_{C8—C9}$	0.98876	49.88	50.12
$\sigma_{C15—N19}$	0.98465	40.01	59.99
$\sigma_{C18—N19}$	0.98498	40.16	59.84
$LP(1)_{N19}$	0.72270		
$LP(1)_{Ti20}$	0.73941		

Table 10. The NBO, and hybridizations of the intramolecular bonds in $Ti_1N_1C_{18}$, at M06-2X/6-311++G**.

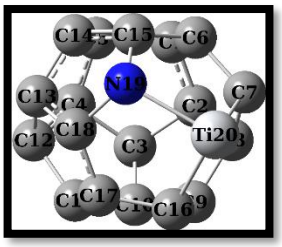

Bond	NBO	s (%)	p (%)	d (%)
$\pi_{C3=C10}$	$0.6589*sp^{99.99}d^{2.69} + 0.7523*sp^{99.99}d^{1.30}$	0.07, 0.08	99.75, 99.81	0.18, 0.11
$\sigma_{C7—Ti20}$	$0.6890*sp^{47.82}d^{0.01} + 0.7247*sp^{0.10}d^{56.24}$	2.05, 1.74	97.93, 0.17	0.03, 98.07
$\sigma_{C8—C9}$	$0.7062*sp^{2.00}d^{0.00} + 0.7080*sp^{1.99}d^{0.00}$	33.28, 33.37	66.64, 66.55	0.08, 0.08
$\sigma_{C15—N19}$	$0.6325*sp^{2.54}d^{0.00} + 0.7745*sp^{2.10}d^{0.00}$	28.21, 32.19	71.67, 67.74	0.13, 0.07
$\sigma_{C18—N19}$	$0.6337* sp^{2.53}d^{0.00} + 0.7736*sp^{2.14}d^{0.00}$	28.29, 31.87	71.59, 68.07	0.13, 0.06
$LP(1)_{N19}$	$sp^{99.99}d^{0.97}$	0.05	99.89	0.05
$LP(1)_{Ti20}$	$sp^{0.08}d^{99.99}$	0.73	0.06	99.21

The first two columns show the type of orbital and occupancy between 0.98876 electrons for $\sigma_{C8—C9}$ bonding orbital with sp^2 hybrid *vs.* 0.72270, and 0.73941 electrons for $LP(1)_{N19}$, $LP(1)_{Ti20}$ lone pairs with $sp^{99.99}d^{0.97}$, and $sp^{0.08}d^{99.99}$ hybrids, correspondingly. The sp^2 hybrid on C_8, and C_9 atoms of C_8—C_9 sigma bond has 33.28, and 33.37% s, 66.64, and 66.55% p-character, respectively. Also, the $sp^{99.99}d^{0.97}$ hybrid on lone pair of N_{19} has 0.05% s, 99.89% p, and 0.05% d-character. While, the $sp^{0.08}d^{99.99}$ hybrid on lone pair of Ti_{20} has 0.73% s, 0.06% p, and 99.21% d-character. The occupancy of $\sigma_{C7—Ti20}$, $\sigma_{C15—N19}$, and $\sigma_{C18—N19}$ is 0.86892, 0.98465, and 0.98498 electrons, with $0.6890*sp^{47.82}+0.7247*sp^{0.10}d^{56.24}$, $0.6325*sp^{2.54}+0.7745*sp^{2.10}$, and $0.6337*sp^{2.53}+0.7736*sp^{2.14}$ hybrid, respectively. Evidently, hetero bonding orbitals of $\sigma_{C7—Ti20}$, $\sigma_{C15—N19}$, and $\sigma_{C18—N19}$ have 47.47% C_7, 40.01% C_{15}, 40.16% C_{18}, 52.53% Ti_{20}, 59.99% N_{19}, and 59.84% N_{19} characters in their corresponding hybrids, respectively. Therefore, titanium and nitrogen heteroatoms have the more percentage of NBOs and gives the more polarization coefficients (0.7247, 0.7745, and 0.7736) than the homo bonding bonds (C—C and/or C═C) because typical titanium has low ability to form hybrid orbitals and prefers $[Ar](4s^2)(3d^2)$ valence electronic configuration which leads to the divalent doublet ground state, and nitrogen has the higher electronegativity than carbon atom. The more important $E^{(2)}$ of $Ti_1N_1C_{18}$ is related to $LP(1)_{N19} \rightarrow \pi^*_{C17=C18}$, $\pi_{C8=C9} \rightarrow \sigma^*_{C7—Ti20}$, $\pi_{C6=C15} \rightarrow \sigma^*_{C7—Ti20}$, $\sigma_{C7—Ti20} \rightarrow \pi^*_{C8=C9}$ and $LP(1)_{N19} \rightarrow \sigma^*_{C7—Ti20}$ orbital's and their corresponding energy is 10.03, 7.07, 6.58, 5.83, and 3.42 kcal/mol, correspondingly (Table 11).

Table 11. The $E^{(2)}$ of the intramolecular bonds in $Ti_1N_1C_{18}$, at M06-2X/6-311++G**.

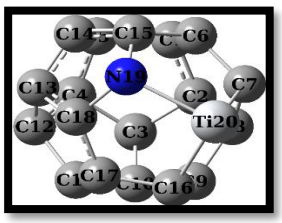

Donor NBO (i)	Acceptor NBO (j)	$E^{(2)}$ (kcal/mol)
$\pi_{C8 = C9}$	$\sigma^*_{C7 — Ti20}$	7.07
$\pi_{C6 = C15}$	$LP^*(2)_{Ti20}$	0.30
$\pi_{C6 = C15}$	$\sigma^*_{C7 — Ti20}$	6.58
$\sigma_{C7 — Ti20}$	$\pi^*_{C8 = C9}$	5.83
$\sigma_{C7 — Ti20}$	$\sigma^*_{C9 — C16}$	0.26
$LP(1)_{N19}$	$\sigma^*_{C7 — Ti20}$	3.42
$LP(1)_{N19}$	$\pi^*_{C17 = C18}$	10.03

These interactions is resulted from the electron donating of the bonding orbitals to the electron acceptoring anti-bonding orbitals, indicating higher CT is happened in these orbitals, compared to lower CT from $\pi_{C6=C15}$ to $LP^*(2)_{Ti20}$, and from $\sigma_{C7—Ti20}$ to $\sigma^*_{C9—C16}$ with $E^{(2)}$ of 0.30, and 0.26 kcal/mol, respectively.

4. Conclusions

Substituent effects of Ti—N units on geometry, $\Delta E_{HOMO\text{-}LUMO}$, ionization potential, aromaticity, NBO charge of C_{20} derivatives are accessed, at DFT. The vibrational frequency calculations imply exclusive of $C_4Ti_8N_8$ species, reminders are real minima and none of analogous collapse to open deformed cage. The $\Delta E_{HOMO\text{-}LUMO}$ of 1.79, 2.06, and 1.80 eV proposes the $C_{18}Ti_1N_1$ as the most kinetic stable and the weakest conductive structure. Also, the $\Delta E_{HOMO\text{-}LUMO}$ of 0.98, 0.82, and 0.97 eV suggests the $C_{12}Ti_4N_4$ with four separated Ti—N units *via* 4 C═C bonds as the least kinetic stable and the strongest conductive system. The calculated IE (IP) of 162.07 kcal/mol, NICS (0) of -42.05 ppm and NICS $(0)_{ZZ}$ of -60.98 ppm display $C_{18}Ti_1N_1$ that in which one Ti—N unit is replaced to two neighboring carbon atoms, as the most thermodynamic stable and the most aromatic nanocage. The most and the least charge on Ti of $C_{18}Ti_1N_1$ (+1.269) and $C_4Ti_8N_8$ (+0.527), also the least and the most $|E_{ads.}|$ of −18.9 and −33.20 kcal/mol, leads to increasing and decreasing capacity of $C_{18}Ti_1N_1$ and $C_4Ti_8N_8$ for hydrogen storage, respectively. Furthermore, in going from $C_{18}Ti_1N_1$ to $C_4Ti_8N_8$, as n increases both nucleophilicity index (N), and chemical potential (μ) increase with $C_{18}Ti_1N_1$ and $C_4Ti_8N_8$ turning out as the least and most nucleophilic species, respectively, while electronegativity (χ) decreases. The MEP maps qualitatively verify the nucleophilicity strength. The NBO analysis of $C_{18}Ti_1N_1$ points out higher ICT including $LP(1)_N \rightarrow \pi^*_{C=C}$, $\pi_{C=C} \rightarrow \sigma^*_{C—Ti}$, $\pi_{C=C} \rightarrow \sigma^*_{C—Ti}$, $\sigma_{C—Ti} \rightarrow \pi^*_{C=C}$ and $LP(1)_N \rightarrow \sigma^*_{C—Ti}$ orbitals.

Acknowledgements

Authors state that no fund is used in this research.

References

[1] (a) M. Koohi, H. Bastami, Structure, stability, MEP, NICS, reactivity, and NBO of Si—Ge nanocages evolved from C_{20} fullerene at DFT. Monatshefte für Chemie – Chem. Mont. 151 (2020) 693. (b) M. Koohi, M. Ghavami, B. N. Haerizade, H. Zandi, M. Z. Kassaee, Cyclacenes and short zigzag nanotubes with alternanting Ge—C bonds: theoretical impacts of Ge on the ground state, strain, and band gap. J. Phys. Org. Chem. 27 (2014) 735. (c) M. T. Baei, M. Koohi, M. Shariati, Characterization of C_{20} fullerene and its isolated $C_{20\text{-}n}Ge_n$ derivatives (n = 1-5) by alternating germanium atom(s) in equatorial position: A DFT survey.

Heteroatom Chem. 29 (2018) e21410. (d) S. Soleimani Amiri, M. Koohi, B. Mirza, Characterizations of B, and N heteroatoms as substitutional doping on structure, stability, and aromaticity of novel heterofullerenesevolvedfrom the smallest fullerene cage C_{20}: A density functional theory perspective. J. Phys. Org. Chem. 29 (2016) 514. (e) M. Koohi, S. Soleimani Amiri, B. N. Haerizade, Substituent effect on structure, stability and aromaticity of novel $B_nN_mC_{20-(n+m)}$ heterofullerenes. J. Phys. Org. Chem. 30 (2017) e3682. (f) M. Koohi, S. Soleimani-Amiri, M. Shariati, Novel X- and Y-substituted heterofullerenes $X_4Y_4C_{12}$ developed from the nanocage C_{20}, where X = B, Al, Ga, Si and Y = N, P, As, Ge: a comparative investigation on their structural, stability, and electronic properties at DFT. Struct. Chem. 29(3) (2018) 909. (g) M. Koohi, M. Shariati, S. Soleimani Amiri, A comparative study on the Ge_6C_{14} heterofullerene nanocages: a density functional survey. J. Phys. Org. Chem. 30 (2017) e3678.

[2] (a) M. Z. Kassaee, F. Boazar, M. Koohi, Heteroatom impacts on structure, stability and aromaticity of X_nC_{20-n} fullerenes: A theoretical prediction, J. Mol. Struct. (Theochem, Comput. Theor. Chem.) 940 (2010) 19. (b) M. T. Baei, M. Koohi, M. Shariati, Structure, stability, and electronic properties of AlP nanocages evolved from the world's smallest caged fullerene C_{20}: A computational study at DFT, J. Mol. Struct. 1159 (2018) 118. (c) M. Koohi, M. Z. Kassaee, M. Ghavami, B. N. Haerizade, A. A. Ahmadi, $C_{20-n}Ge_n$ heterofullerenes (n = 5 - 10) on focus: A density functional perspective, Monatsh. Chem. 146 (2015) 1409. (d) M. Koohi, S. Soleimani Amiri, M. Shariati, Silicon impacts on structure, stability and aromaticity of $C_{20-n}Si_n$ heterofullerenes (n = 1 - 10): A density functional perspective, J. Mol. Struct. 1127 (2017) 522.

[3] (a) E. Vessally, S. A. Siadati, A. Hosseinian, L. Edjlali, Selective sensing of ozone and the chemically active gaseous species of the troposphere by using the C_{20} fullerene and graphene segment, Talanta 162 (2017) 505. (b) E. Vessally, S. Soleimani–Amiri, A. Hosseinian, L. Edjlali, A. Bekhradnia, The Hartree–Fock exchange effect on the CO adsorption by the boron nitride nanocage, Physica E 87 (2017) 308. (c) L. Safari, E. Vessally, A. Bekhradnia, A. Hosseinian, L. Edjlali, A DFT study on the sensitivity of two–dimensional BN nanosheet to nerve agents cyclosarin and tabun, Thin Solid Films 623 (2017) 157. (d) S. A. Siadati, E. Vessally, A. Hosseinian, L. Edjlali, Possibility of sensing, adsorbing, and destructing the Tabun–2D–skeletal (Tabun nerve agent) by C_{20} fullerene and its boron and nitrogen doped derivatives, Synthetic. Met. 220 (2016) 606. (e) E. Vessally, S. Soleimani–Amiri, A. Hosseinian, L. Edjlali, A. Bekhradnia, A comparative computational study on the BN ring doped nanographenes, Appl. Surf. Sci. 396 (2017) 740.

[4] (a) E. Vessally, F. Behmagham, B. Massoumi, A. Hosseinian, L. Edjlali, Carbon nanocone as an electronic sensor for HCl gas: Quantum chemical analysis, Vacuum 134 (2016) 40. (b) S. Bashiri, E. Vessally, A. Bekhradnia, A. Hosseinian, L. Edjlali, Utility of extrinsic [60] fullerenes as work function type sensors for amphetamine drug detection: DFT studies, Vacuum 136 (2017) 156. (c) F. Behmagham, E. Vessally, B. Massoumi, A. Hosseinian, L. Edjlali, A computational study on the SO_2 adsorption by the pristine, Al, and Si doped BN nanosheets, Superlattices Microstruct. 100 (2016) 350.

[5] Q. Feng, Y. Li, N. Wang, Y. Hao, J. Chang, Z. Wang, X. Zhang, Z. Zhang, L. Wang, A Biomimetic Nanogenerator of Reactive Nitrogen Species Based on Battlefield Transfer Strategy for Enhanced Immunotherapy, Small 16 (2020) e2002138.

[6] L. He, J. Liu, Y. Liu, B. Cui, B. Hu, M. Wang, Z. Peng, Titanium dioxide encapsulated carbon-nitride nanosheets derived from MXene and melamine-cyanuric acid composite as a multifunctional electrocatalyst for hydrogen and oxygen evolution reaction and oxygen reduction reaction, Appl. Cat. B: Env. 248 (2019) 366.

[7] (a) E. Vessally, M. D. Esrafili, R. Nurazar, P. Nematollahi, A. Bekhradnia, A DFT study on electronic and optical properties of aspirin–functionalized $B_{12}N_{12}$ fullerene–like nanocluster, Struct. Chem. 28 (2017) 735. (b) E. Vessally, E. Ahmadi, S. Alibabaei, M. D. Esrafili, A. Hosseinian, Adsorption and decomposition of formaldehyde on the $B_{12}N_{12}$ nanostructure: a density functional theory study, Monatsh. Chem. 148 (2017) 1727. (c) K. Nejati, A. Hosseinian, E. Vessally, A. Bekhradnia, L. Edjlali, A theoretical study on the electronic sensitivity of the pristine and Al-doped $B_{24}N_{24}$ nanoclusters to F_2CO and Cl_2CO gases, Struct. Chem. 28 (2017) 1919.

[8] (a) M. Bertau, F. Wahl, A. Weiler, K. Scheumann, J. Worth, M. Keller, H. Prinzbach, From Pagodanes to Dodecahedranes - Search for a Serviceable Access to the Parent (C20H20) Hydrocarbon, Tetrahedron 53 (1997) 10029. (b) H. Prinzbach, A. Weiler, P. Landenberger, F. Wahl, J. Worth, L. T. Scott, M. D. Gelmont, D. Olevano, B. V. Issendorff, Gas-Phase Production and Photoelectron Spectroscopy of the Smallest Fullerene, C_{20}, Nature 407 (2000) 60.

[9] S. Soleimani-Amiri, M. Koohi, Z. Azizi, Characterization of nonsegregated $C_{17}Si_3$ heterofullerenic isomers using density functional theory method, J. Chin. Chem. Soc. 65 (2018) 1453.

[10] (a) J. M. Campanera, C. Bo, J. M. Poblet, General Rule for the Stabilization of Fullerene Cages Encapsulating Trimetallic Nitride Templates, Angew. Chem., Int. Ed. 44 (2005) 7230. (b) J. C. Gonzalez, S. Mondal, F. Ocayo, R. Guajardo-Maturana, A. Muñoz-Castro, Nature of C_{60} and C70 fullerene encapsulation in a porphyrin- and metalloporphyrin-based cage: Insights from dispersion-corrected density functional theory calculations, Int. J. Quantum Chem. 120 (2019) e26080. (c) F. A. Shakib, M. R. Momeni, Density functional investigation of metal encapsulated $X@C_{12}Si_8$ heterofullerene (Li^+, Na^+, K^+, Be^{2+}, Mg^{2+}, Ca^{2+}, Al^{3+}, Ga^{3+}), Physica B 406 (2011) 1471.

[11] (a) S. A. Siadati, E. Vessally, A. Hosseinian, L. Edjlali, Possibility of sensing, adsorbing, and destructing the Tabun–2D–skeletal (Tabun nerve agent) by C_{20} fullerene and its boron and nitrogen doped derivatives. Synthetic Met 220 (2016) 606. (b) E. Vessally, S. A. Siadati, A. Hosseinian, L. Edjlali, Selective sensing of

ozone and the chemically active gaseous species of the troposphere by using the C_{20} fullerene and graphene segment. Talanta 162 (2017) 505. (c) E. Vessally, S. Soleimani–Amiri, A. Hosseinian, L. Edjlali, A. Bekhradnia, The Hartree–Fock exchange effect on the CO adsorption by the boron nitride nanocage. Physica E 87 (2017) 308. (d) K. Nejati, A. Hosseinian, E. Vessally, A. Bekhradnia, L. Edjlali, A comparative DFT study on the interaction of cathinone drug with BN nanotubes, nanocages, and nanosheets. Appl. Surf. Sci. 422 (2017) 763. (e) A. Hosseinian, E. Vessally, A. Bekhradnia, K. Nejati, G. Rahimpour, Benzoylethanamine drug interaction with the AlN nanosheet, nanotube and nanocage: Density functional theory studies. Thin Solid Films 640 (2017) 93.

[12] P. W. Dunk, N. K. Kaiser, M. Mulet-Gas, A. Rodríguez-Fortea, J. M. Poblet, H. Shinohara, C. L. Hendrickson, A. G. Marshall, H. W. Kroto, The Smallest Stable Fullerene, M@C_{28} (M = Ti, Zr, U): Stabilization and Growth from Carbon Vapor, J. Am. Chem. Soc. 134 (2012) 9380.

[13] H. Dong, T. Hou, S.-T. Lee, Y. Li, New Ti-decorated B_{40} fullerene as a promising hydrogen storage material, Sci. Reports 5 (2015) 9952.

[14] (a) A. Hassanpour, P. Delir Kheirollahi Nezhad, A. Hosseinian, A. G. Ebadi, S. Ahmadi, S. Ebrahimiasl, Characterization of IR spectroscopy, APT charge, ESP maps and AIM analysis of C_{20} and its $C_{20-n}Al_n$ heterofullerene analogous (n = 1 - 5) using DFT, J. Phys. Org. Chem. 34 (7) (2021) e4198. (b) K. Nejati, A. Hosseinian, L. Edjlali, E. Vessally, The effect of structural curvature on the cell voltage of BN nanotube based Na–ion batteries, J. Mol. Liq. 229 (2017) 167. (c) L. Safari, E. Vessally, A. Bekhradnia, A. Hosseinian, L. Edjlali, A DFT study on the sensitivity of two–dimensional BN nanosheet to nerve agents cyclosarin and tabun. Thin Solid Films, 623 (2017) 157. (d) A. Hassanpour, L. Youseftabar-Miri, P. Delir Kheirollahi Nezhad, S. Ahmadi, S. Ebrahimiasl, Kinetic stability, and NBO analysis of the $C_{20-n}Al_n$ nanocages (n = 1 - 5) using DFT investigation, J. Mol. Struct. 1233 (2021) 130079. (e) A. Hassanpour, S. Yasar, A. G. Ebadi, S. Ebrahimiasl, S. Ahmadi, Thermodynamic stability, structural and electronic properties for the $C_{20-n}Al_n$ heterofullerenes (n = 1 - 5): A DFT study, J. Mol. Model. (2021) DOI: 10.1007/s00894- 021-04727-y.

[15] P. Liu, H. Zhang, X. Cheng, Y. Tang, Ti-decorated B_{38} fullerene: A high capacity hydrogen storage material, Int. J. Hydrogen Energy 41 (2016) 19123.

[16] (a) A. D. Becke, Density-functional exchange-energy approximation with correct asymptotic behavior, Phys. Rev. A 38 (1988) 3098. (b) A. D. J. Becke, Density-functional thermochemistry. III. The role of exact exchange, Chem. Phys. 98 (1993) 5648. (c) C. Lee, W. Yang, R. G. Parr, Development of the Colle-Salvetti correlation-energy formula into a functional of the electron density, Phys. Rev. B 37 (1988) 785. (d) A. D. Becke, Density-functional thermochemistry. IV. A new dynamical correlation functional and implications for exact-exchange mixing, J. Chem. Phys. 104 (1996) 1040.

[17] (a) M. W. Schmidt, K. K. Baldridge, J. A. Boatz, S. T. Elbert, M. S. Gordon, J. H. Jensen, S. Koseki, N. Matsunaga, K. A. Nguyen, S. J. Su, T. L. Windus, M. Dupuis, J. A. Montgomery, General atomic and molecular electronic structure system, J. Comput. Chem., 14 (11) (1993) 1347. (b) A. L. Sobolewski, W. Domcke, *Ab Initio* Investigation of the Structure and Spectroscopy of Hydronium−Water Clusters, J. Phys. Chem. A 106 (2002) 4158.

[18] (a) W. J. Hehre, L. Radom, P. v. R. Schleyer, J. A. Pople, *Ab Initio* Molecular Orbital Theory, John Wiley & Sons, New York (1986). (b) J. B. Foresman, A. Frisch, Exploring Chemistry with Electronic structure Methods, Gaussian, Inc., Pittsburgh. PA (1996).

[19] (a) F. Weinhold, E. D. Glendening, NBO 7.0 Program Manual Natural Bond Orbital Analysis Programs. J. Comput. Chem. 33 (2012) 2363. (b) E. D. Glendening, C. R. Landis, F. Weinhold, Natural bond orbital methods. Wiley Interdiscip. Rev. Comput. Mol. Sci. 2 (2012) 1.

[20] (a) P. v. R. Schleyer, C. Maerker, A. Dransfeld, H. Jiao, N. J. R. van Eikema Hommes, Nucleus-independent chemical shifts (NICS): a simple and efficient aromaticity probe. J. Am. Chem. Soc. 118 (1996) 6317. (b) P. v. R. Schleyer, H. Jiao, N. J. R. van Eikema Hommes, V. G. Malkin, O. L. Malkina, An evolution of the aromaticity of inorganic rings: refined evidence from magnetic properties. J Am Chem Soc 119 (1997) 12669. (c) P. v. R. Schleyer, M. Manoharan, Z. Wang, B. Kiran, H. Jiao, R. Puchta, N. J. R. van Eikema Hommes, Dissected nucleus-independent chemical shift analysis of p-aromaticity and antiaromaticity. Org. Lett. 3(16) (2001) 2465.

[21] a) L. R. Domingo, E. Chamorro, P. Pérez, Understanding the Reactivity of Captodative Ethylenes in Polar Cycloaddition Reactions. A Theoretical Study. J Org Chem 73 (2008) 4615. (b) R. G. Parr, L. Szentpaly, S. Liu, Electrophilicity Index. J. Am. Chem. Soc. 121 (1999) 1922. (c) R. G. Pearson Absolute electronegativity and hardness: applications to organic chemistry. J. Org. Chem. 54 (1989) 1423. (d) P. K. Chattaraj, S. Giri, Stability, Reactivity, and Aromaticity of Compounds of a Multivalent Superatom. J. Phys. Chem. A 111 (2007) 11116. (e) J. Padmanabhan, R. Parthasarathi, V. Subramanian, P. K. Chattaraj, Electrophilicity-Based Charge Transfer Descriptor. J. Phys. Chem. A 111 (2007) 1358.

[22] a) R. C. Haddon, L. T. Scott, π-Orbital Conjugation and Rehybridization in Bridged Annulenes and Deformed Molecules in General: π-Orbital Axis Vector Analysis. Pure Appl. Chem. 58 (1986) 137. (b) R. C. Haddon, Chemistry of the fullerenes: The manifestation of strain in a class of continuous aromatic molecules. Science 261 (1993) 1545. (c) T. Lin, W.-D. Zhang, J. Huang, C. He, A DFT Study of the Amination of Fullerenes and Carbon Nanotubes: Reactivity and Curvature. J. Phys. Chem. B 109 (2005) 13755. (d) H. Prinzbach, A. Weller, P. Landenberger, F. Wahl, J. Worth, L. T. Scott, M. Gelmont, D. Olevano, B. Issendorff, Gas-Phase Production and Photoelectron Spectroscopy of the Smallest Fullerene, C_{20}. Nature 407 (2000) 60. (e) Z. Chen, T. Heine, H. Jiao, A. Hirsch, W. Thiel, P. v. R.

Schleyer, Theoretical Studies on the Smallest Fullerene: From Monomer to Oligomers and Solid States. Chem. Eur. J. 10 (2004) 963. (f) A. Hirsch, Z. Chen, H. Jiao, Spherical Aromaticity in I_h Symmetrical Fullerenes: The $2(N+1)^2$ Rule. Angew. Chem. Int. Ed. 39 (2000) 3915–3917. (g) M. N. Huda, A. K. Ray, Evolution of SiC nanocluster from carbon fullerene, a density functional theoretic study. Chem. Phys. Lett. 457 (2008) 124. (h) R. W. Alder, M. E. Blake, J. M. Oliva, Diaminocarbenes; Calculation of Barriers to Rotation about $C_{carbene}$-N Bonds, Barriers to Dimerization, Proton Affinities and ^{13}C NMR Shifts. J. Phys. Chem. A 103 (1999) 11200.

[23] (a) G. E. Froudakis, Why alkali-metal-doped carbon nanotubes possess high hydrogen uptake, Nano. Lett. 1 (2001) 531. (b) A. Mavrandonakis, G. E. Froudakis, M. Schnell, M. Muhlhauser, From pure carbon to silicon carbon nanotubes: an *ab initio* study, Nano. Lett. 3 (2003) 1481. (c) G. Mpourmpakis, G. E. Froudakis, G. P. Lithoxoos, J. Samios, SiC nanotubes: a novel material for hydrogen storage, Nano. Lett. 6 (2006) 158